ChemComm

COMMUNICATION

View Article Online
View Journal | View Issue

Cite this: *Chem. Commun.*, 2023, **59**, 10024

Received 30th June 2023,
Accepted 26th July 2023

DOI: 10.1039/d3cc03172a

rsc.li/chemcomm

Facile solid-state synthesis of a layered Co-free, Ni-rich cathode material for all-solid-state batteries†

Saravanakumar Murugan,*[a] Ruizhuo Zhang,[a] Jürgen Janek,[ab] Aleksandr Kondrakov[ac] and Torsten Brezesinski*[a]

Layered Ni-rich oxides are attractive cathode active materials for secondary battery applications. Combining them with inorganic superionic conductors and high-capacity anodes can significantly increase energy density. Herein we successfully synthesized spherical secondary particles of a Mn-substituted $LiNiO_2$, $LiNi_{0.95}Mn_{0.05}O_2$ (a Co-free NMX material), for use in bulk-type lithium-thiophosphate-based all-solid-state batteries.

The exponential growth in the demand for electric vehicles necessitates a shift in energy-storage systems. The primary energy-storage systems used for electric vehicles are secondary batteries, with lithium-ion batteries (LIBs) currently dominating the market. However, achieving high energy density with conventional LIBs is limited both by the storage capacity of the active materials and by the additional weight and volume of the inactive components (separator, electrolyte *etc.*). Furthermore, the use of flammable electrolyte solvent(s) can pose a safety risk. As a result, alternative technologies are sought after. All-solid-state batteries (ASSBs) utilizing inorganic materials that serve as the separator and superionic electrolyte, among others, could potentially increase energy density and reduce the risk of fire hazards/dendrite formation during cycling.[1–6]

Layered Ni-rich oxide cathode active materials (CAMs) of type $LiNi_xCo_yMn_{1-x-y}O_2$ (NCM or NMC) have been commercialized because of their high specific capacity and favorable working potential. Although Co is advantageous due to its contribution towards high conductivity and structural stability, the downside of cobalt sourcing and its toxicity have led to the advancement of Co-free cathodes (usually referred to as NMX).[7,8] Apart from that, the CAM synthesis requires the use of various salts and bases during the precipitation reaction in order to obtain a well-defined (and highly pure) material. This demands precise control over precursor morphology, washing and drying, which ultimately affects the overall cost.[9,10] For ASSBs, careful considerations need to be taken in the design of the CAM. Superionic lithium thiophosphate solid electrolytes (SEs), in particular, are prone to interfacial side reactions due to their relatively poor electrochemical stability. To mitigate (or ideally prevent) SE degradation upon cycling, various coating materials have been applied to the CAM particles aiming at preventing direct contact with the SE.[11,12]

NMX cathodes produced by co-precipitation and subsequent calcination in the presence of a lithium source have already been shown to exhibit promising performances in LIBs.[13] In this study, a layered Co-free, Ni-rich CAM, $LiNi_{0.95}Mn_{0.05}O_2$, referred to as NMX9505 hereafter, was prepared by solid-state synthesis, and a $LiNbO_3$ protective nanocoating was applied to the surface of the secondary particles by sol–gel chemistry. The resulting material was electrochemically tested in ASSB cells by stacking NMX9505 cathode, argyrodite Li_6PS_5Cl (LPSCl) SE separator and $Li_4Ti_5O_{12}$ (LTO) anode (see Experimental section in the ESI† for details). The coated NMX9505 delivered high specific capacities of 164 mA h g^{-1} at 0.2C (137 mA h g^{-1} for uncoated CAM) and 86 mA h g^{-1} at 2C (36 mA h g^{-1} for uncoated CAM) and retained 77% of the initial capacity (190 mA h g^{-1} at 0.1C) after 81 cycles (rate performance testing at 0.1, 0.2, 0.5, 1 and 2C with five cycles each, followed by 0.2C cycling), compared to 68% for uncoated CAM. The cell resistance was determined by electrochemical impedance spectroscopy (EIS) and *post mortem* analysis was carried out using cross-sectional scanning electron microscopy (SEM).

The NMX9505 material employed in this work displayed a typical polycrystalline morphology, characterized by the formation of secondary particles that are predominantly spherical

[a] *Battery and Electrochemistry Laboratory (BELLA), Institute of Nanotechnology, Karlsruhe Institute of Technology (KIT), Hermann-von-Helmholtz-Platz 1, Eggenstein-Leopoldshafen 76344, Germany. E-mail: saravanakumar.murugan@kit.edu, torsten.brezesinski@kit.edu*
[b] *Institute of Physical Chemistry and Center for Materials Research, Justus-Liebig-University Giessen, Heinrich-Buff-Ring 17, Giessen 35392, Germany*
[c] *BASF SE, Carl-Bosch-Str. 38, Ludwigshafen 67056, Germany*

† Electronic supplementary information (ESI) available: Experimental section, SEM images, voltage profiles, differential capacity curves, impedance analysis and ICP-OES results. See DOI: https://doi.org/10.1039/d3cc03172a

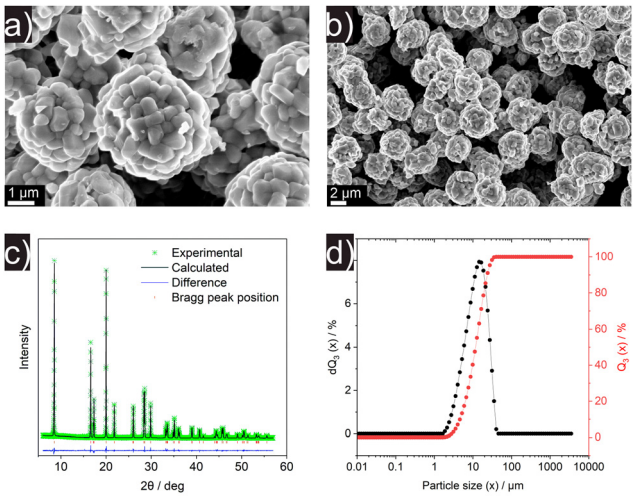

Fig. 1 Characterization of the as-prepared NMX9505 CAM. (a) and (b) SEM images at different magnifications, (c) XRD pattern and corresponding Rietveld refinement profile (R_{wp} = 10.38%, reduced χ^2 = 0.98; ICSD card no. 152273) and (d) particle size distribution.

in shape. The latter shape is a direct result of the inherent morphology of the 4 µm diameter $Ni(OH)_2$ precursor used in the synthesis [SEM images of the $Ni(OH)_2$ and Mn_2O_3 nanoparticle precursors are shown in Fig. S1, ESI†]. In contrast, $LiOH{\cdot}H_2O$ tends to melt during calcination, while Mn_2O_3 remains in nano-sized form. Overall, the NMX9505 secondary particles are the product of the sintering process that occurs between numerous primary particles (see SEM images at different magnifications in Fig. 1a and b). Fig. 1c presents the powder X-ray diffraction (XRD) pattern and corresponding Rietveld refinement profile for the as-prepared NMX9505 CAM. The material revealed the expected layered structure derived from α-$NaFeO_2$ (O3 type, $R\bar{3}m$ space group) and was free of crystalline impurity phases.[14] The refined lattice parameters are $a = b = 2.87848(13)$ Å, $c = 14.21664(54)$ Å, with cell volume $V = 102.013(6)$ Å^3, similar to NMX materials synthesized from a co-precipitated precursor CAM.[15] Also, the c/a ratio equals 4.94, indicating that the NMX9505 exhibits a well-ordered (layered) structure.[16] The presence of Mn^{4+} leads to the formation of an equal amount of Ni^{2+} ions in the lattice, which migrate to the lithium layer due to size similarity [$r(Ni^{2+})$ = 0.69 Å *vs.* $r(Li^+)$ = 0.76 Å).[17] Note that the Li^+ ions may also migrate to the transition-metal layer, ultimately leading to Li/Ni intermixing (formation of Ni_{Li} and Li_{Ni} defects).[18,19] Rietveld analysis revealed a site disorder (Ni_{Li}) of about 3%, which is lower than that of a NMX material of ''same'' composition reported previously.[20]

Results from inductively coupled plasma-optical emission spectroscopy (ICP-OES) measurements (see Table S1, ESI†) indicated that the Li, Ni and Mn contents in the NMX9505 CAM are close to the targeted stoichiometry of $LiNi_{0.95}Mn_{0.05}O_2$. This demonstrates that the solid-state synthesis approach used in the present work has no major effect on the final composition. Particle size distribution analysis *via* laser diffraction further revealed d_{10}, d_{50} and d_{90} values of 5.27, 13.3 and 26.6 µm, respectively (see Fig. 1d).

At first, the as-prepared NMX9505 [7.5 (±0.5) mg cm^{-2} loading] was electrochemically tested in LIB half-cells at room temperature (25 °C) in the potential window of 2.7–4.3 V *vs.* Li^+/Li in order to examine its cycling performance. Fig. 2a shows the specific discharge capacity *versus* the cycle number for different C-rates (0.2, 0.5, 1, 2 and 5C with five cycles each, followed by 0.2C cycling). The initial specific discharge capacity at 0.2C (200 mA h g^{-1}, 1.5 mA h cm^{-2}) was largely recovered in the 26th cycle (97%), despite the rate performance testing at the beginning of cycling. Also, the material was capable of delivering high specific capacities at high C-rates, with $q_{dis} \approx 161$ mA h g^{-1} at 2C and 129 mA h g^{-1} at 5C. Fig. 2b presents the long-term cycling of the CAM at 1C. The coin cells exhibited a high initial specific discharge capacity of 210 mA h g^{-1} at 0.1C and maintained an average Coulomb efficiency of 99.9%, with a capacity decay rate of 0.097% per cycle (from the 3rd cycle with $q_{dis} \approx$ 187 mA h g^{-1} to the 250th cycle with 142 mA h g^{-1}). With regards to capacity and stability (capacity retention), the NMX9505 employed here clearly outperforms a previously reported material with similar composition and polycrystalline morphology.[15]

Interfacial degradation in lithium-thiophosphate-based ASSBs has been shown to negatively affect cell performance.[21–24] Amorphous $LiNbO_3$, a widely used (inert) coating material for CAMs, can mitigate adverse side reactions and improve cyclability.[11,25–27] Here, the NMX9505 CAM was coated with a thin shell of sol–gel derived $LiNbO_3$ (1 wt%), as described in the Experimental section of the ESI.† Bulk-type ASSB cells were assembled with LPSCl and LTO serving as SE (in the cathode, anode and separator) and anode, respectively, and then subjected to galvanostatic charge/discharge testing at elevated temperature (45 °C) in the voltage range between 1.15 and 2.75 V *vs.* $Li_4Ti_5O_{12}$/$Li_7Ti_5O_{12}$ (around 2.7–4.3 V *vs.* Li^+/Li).

Fig. 2c shows a comparison of the cycling performance between coated and uncoated NMX9505 [10.5 (±0.5) mg cm^{-2} loading]. Overall, the coated CAM delivered higher capacities

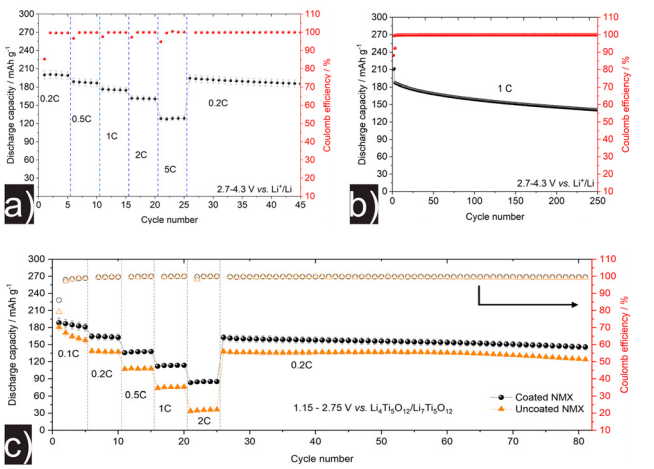

Fig. 2 Electrochemical analysis of the $LiNbO_3$-coated and uncoated NMX9505 CAMs in (a), (b) LIB (at 25 °C) and (c) ASSB cells (at 45 °C). 1C is defined as a specific current of 200 mA g^{-1}. Data from two independent cells are shown. If error bars are not visible, they are smaller than the symbols.

and further showed improved rate capability over the uncoated material. For example, the initial specific discharge capacity was 189 mA h g^{-1} (2 mA h cm^{-2}) at 0.1C, with a first-cycle Coulomb efficiency of 86%. The capacity retention after 81 cycles (including rate performance testing and subsequent cycling at 0.2C) was 77%. In contrast, uncoated NMX9505 exhibited an initial specific discharge capacity of 181 mA h g^{-1} at 0.1C, with only 79% Coulomb efficiency. A large difference in capacity was observed for the uncoated CAM, which only delivered 35 mA h g^{-1} at 2C, compared to 85 mA h g^{-1} for the surface-treated NMX9505, evidencing that the protective coating improves rate performance and reversibility by stabilizing the CAM/SE interface. Similarly, uncoated CAM only retained 68% of its initial capacity.

The severity of the voltage hysteresis (overpotential) is visualized in Fig. S2 (ESI†). It is worth noting that the overpotential increased more significantly for the uncoated than coated NMX9505 with increasing C-rate. An increase in overpotential is indicative of side reactions and unstable cathode interface (cell impedance buildup). Additionally, differential capacity (dq/dV) curves comparing both CAMs in the 1st (0.1C), 23rd (2C) and 81st (0.2C) cycle are presented in Fig. S3 (ESI†). While the materials undergo similar phase transitions [from H1 (hexagonal) to M (monoclinic) at around 2.1 V, M to H2 at 2.5 V and H2 to H3 at 2.7 V] in the initial cycle at 0.1C, they are strongly suppressed at high C-rates (23rd cycle), leading to reduced capacity, especially for the uncoated NMX9505. Also, in the 81st cycle, the latter CAM showed suppressed H2–H3 transition and peak shifts during charge and discharge, thus indicating increased polarization, presumably due to unwanted side reactions and mechanical degradation.[28,29]

To further probe into the origin of the increase in polarization, EIS measurements were conducted on ASSB cells with the coated and uncoated NMX9505 cathodes at 45 °C. Nyquist plots of the electrochemical impedance before cycling and after the 81st cycle (discharged state) are shown in Fig. 3. Qualitative analysis revealed insignificant differences between both CAMs in the pristine state. However, after 81 cycles, two semicircles appeared at high and medium frequencies. By comparing the cathode interface resistance (medium frequencies), it was found that the coated CAM exhibits a significantly lower $R_{CAM|SE}$, about less than half that of the uncoated material.

Fig. S4 (ESI†) plots the real part of the impedance *versus* the reciprocal root square of the frequency. As is evident from the data, the coating has a profound effect on cell impedance; in particular, the resistance at low frequencies was decreased in half. We note that contact loss between the CAM and SE particles is enhanced if there is chemo-mechanical degradation occurring during battery operation.[30–32] This in turn increases the Warburg coefficient [σ; see eqn (S1) and (S2), ESI†], which shows an inverse relationship with the contact area at the interface. Overall, this means that the σ will be lower (enhanced Li-ion diffusion) if there is intimate contact between the individual particles in the electrode.[33,34] However, the slight disparity in σ between the uncoated (13.4 Ω $s^{-1/2}$) and coated NMX9505 (10.8 Ω $s^{-1/2}$) makes it difficult to uncover any minor cracking or contact loss.

For this reason, cross-sectional SEM images were collected from both cathode composites before and after cycling (see Fig. S5, ESI†). No inter- and intraparticle cracking was observed for either coated or uncoated NMX9505 in the pristine state. However, there was a noticeable difference in intensity of particle fracture after cycling, with only the uncoated CAM showing signs of mechanical degradation. While the SEM images shed some light on the effect that the coating has on the cracking behavior, it is important to note that this is not the only factor affecting the performance of the material. Further in-depth surface (and bulk) analysis is necessary to investigate the role of side reactions and local chemical environment in the cyclability of the NMX9505 CAM.[35–38]

Taken together, the current work successfully synthesized a layered Co-free, Ni-rich cathode active material of well-defined (industrially relevant) morphology *via* a facile solid-state reaction route, eliminating the need for conventional co-precipitation routes for introducing manganese. This simplified preparation method also allows for tailoring of the final stoichiometry without the requirement of producing customized precursor cathode materials first. X-ray diffraction analysis revealed a well-layered structure having a relatively low defect density (cation intermixing, off-stoichiometry). The as-prepared NMX9505 material exhibited good performance as the cathode for room-temperature lithium-ion batteries. Based on these results, a $LiNbO_3$ protective nanocoating was applied to the free surface of the NMX9505 secondary particles, followed by testing in all-solid-state battery cells with an argyrodite Li_6PS_5Cl solid electrolyte. The coated material showed superior rate capability and cycling stability over the as-prepared (uncoated) NMX9505, due to suppression of detrimental side reactions and reduced particle fracture. These preliminary data indicate that NMX materials are promising candidates for use in Li-ion batteries with liquid and solid electrolytes.

This work was partially supported by BASF SE. The authors are grateful to Philipp Quarz (Thin Film Technology, KIT) for particle size distribution measurements.

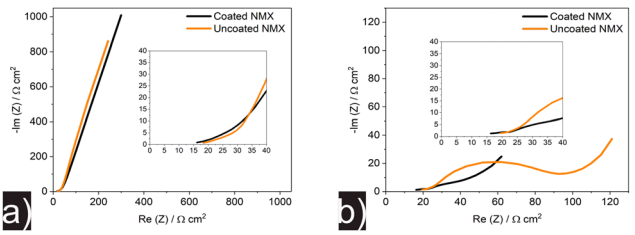

Fig. 3 Impedance analysis of the $LiNbO_3$-coated and uncoated NMX9505 CAMs in ASSB cells (a) before cycling and (b) after 81 cycles (in discharged state) at 45 °C.

Conflicts of interest

There are no conflicts to declare.

Notes and references

1 M. Ma, M. Zhang, B. Jiang, Y. Du, B. Hu and C. Sun, *Mater. Chem. Front.*, 2023, **7**, 1268–1297.
2 C. Wang, J. Liang, Y. Zhao, M. Zheng, X. Li and X. Sun, *Energy Environ. Sci.*, 2021, **14**, 2577–2619.
3 F. Zheng, M. Kotobuki, S. Song, M. O. Lai and L. Lu, *J. Power Sources*, 2018, **389**, 198–213.
4 S. Chen, K. Wen, J. Fan, Y. Bando and D. Golberg, *J. Mater. Chem. A*, 2018, **6**, 11631–11663.
5 L. Fan, S. Wei, S. Li, Q. Li and Y. Lu, *Adv. Energy Mater.*, 2018, **8**, 1702657.
6 J. Wu, L. Shen, Z. Zhang, G. Liu, Z. Wang, D. Zhou, H. Wan, X. Xu and X. Yao, *Electrochem. Energy Rev.*, 2021, **4**, 101–135.
7 N. Voronina, Y.-K. Sun and S.-T. Myung, *ACS Energy Lett.*, 2020, **5**, 1814–1824.
8 J.-H. Kim, K.-J. Park, S. J. Kim, C. S. Yoon and Y.-K. Sun, *J. Mater. Chem. A*, 2019, **7**, 2694–2701.
9 A. S. Wijareni, H. Widiyandari, A. Purwanto, A. F. Arif and M. Z. Mubarok, *Energies*, 2022, **15**, 5794.
10 M. Hietaniemi, T. Hu, J. Välikangas, J. Niittykoski and U. Lassi, *J. Appl. Electrochem.*, 2021, **51**, 1545–1557.
11 S. Payandeh, F. Strauss, A. Mazilkin, A. Kondrakov and T. Brezesinski, *Nano Res. Energy*, 2022, **1**, e9120016.
12 P. Minnmann, F. Strauss, A. Bielefeld, R. Ruess, P. Adelhelm, S. Burkhardt, S. L. Dreyer, E. Trevisanello, H. Ehrenberg, T. Brezesinski, F. H. Richter and J. Janek, *Adv. Energy Mater.*, 2022, **12**, 2201425.
13 Y.-K. Sun, D.-J. Lee, Y. J. Lee, Z. Chen and S.-T. Myung, *ACS Appl. Mater. Interfaces*, 2013, **5**, 11434–11440.
14 Y. S. Meng, G. Ceder, C. P. Grey, W.-S. Yoon, M. Jiang, J. Bréger and Y. Shao-Horn, *Chem. Mater.*, 2005, **17**, 2386–2394.
15 L. Ni, R. Guo, S. Fang, J. Chen, J. Gao, Y. Mei, S. Zhang, W. Deng, G. Zou, H. Hou and X. Ji, *eScience*, 2022, **2**, 116–124.
16 H. Z. Zhang, C. Liu, D. W. Song, L. Q. Zhang and L. J. Bie, *J. Mater. Chem. A*, 2017, **5**, 835–841.
17 R. D. Shannon, *Acta Cryst.*, 1976, **A32**, 751–767.
18 M. Guilmard, L. Croguennec and C. Delmas, *J. Electrochem. Soc.*, 2003, **150**, A1287–A1293.
19 L. Karger, D. Weber, D. Goonetilleke, A. Mazilkin, H. Li, R. Zhang, Y. Ma, S. Indris, A. Kondrakov, J. Janek and T. Brezesinski, *Chem. Mater.*, 2023, **35**, 648–657.
20 D. Goonetilleke, F. Riewald, A. O. Kondrakov, J. Janek, T. Brezesinski and M. Bianchini, *J. Phys. Chem. C*, 2022, **126**, 16952–16964.
21 S. P. Culver, R. Koerver, W. G. Zeier and J. Janek, *Adv. Energy Mater.*, 2019, **9**, 1900626.
22 S. Wang, R. Fang, Y. Li, Y. Liu, C. Xin, F. H. Richter and C.-W. Nan, *J. Materiomics*, 2021, **7**, 209–218.
23 M. B. Dixit, N. Singh, J. P. Horwath, P. D. Shevchenko, M. Jones, E. A. Stach, T. S. Arthur and K. B. Hatzell, *Matter*, 2020, **3**, 2138–2159.
24 Y. Zhu, X. He and Y. Mo, *ACS Appl. Mater. Interfaces*, 2015, **7**, 23685–23693.
25 F. Walther, F. Strauss, X. Wu, B. Mogwitz, J. Hertle, J. Sann, M. Rohnke, T. Brezesinski and J. Janek, *Chem. Mater.*, 2021, **33**, 2110–2125.
26 N. Ohta, K. Takada, I. Sakaguchi, L. Zhang, R. Ma, K. Fukuda, M. Osada and T. Sasaki, *Electrochem. Commun.*, 2007, **9**, 1486–1490.
27 A. Banerjee, X. Wang, C. Fang, E. A. Wu and Y. S. Meng, *Chem. Rev.*, 2020, **120**, 6878–6933.
28 F. Wu, N. Liu, L. Chen, Y. Su, G. Tan, L. Bao, Q. Zhang, Y. Lu, J. Wang, S. Chen and J. Tan, *Nano Energy*, 2019, **59**, 50–57.
29 X. Li, L. Jin, D. Song, H. Zhang, X. Shi, Z. Wang, L. Zhang and L. Zhu, *J. Energy Chem.*, 2020, **40**, 39–45.
30 S. H. Jung, U.-H. Kim, J.-H. Kim, S. Jun, C. S. Yoon, Y. S. Jung and Y.-K. Sun, *Adv. Energy Mater.*, 2020, **10**, 1903360.
31 S. Payandeh, C. Njel, A. Mazilkin, J. H. Teo, Y. Ma, R. Zhang, A. Kondrakov, M. Bianchini and T. Brezesinski, *Adv. Mater. Interfaces*, 2023, **10**, 2201806.
32 R. Ruess, S. Schweidler, H. Hemmelmann, G. Conforto, A. Bielefeld, D. A. Weber, J. Sann, M. T. Elm and J. Janek, *J. Electrochem. Soc.*, 2020, **167**, 100532.
33 J. H. Teo, F. Strauss, F. Walther, Y. Ma, S. Payandeh, T. Scherer, M. Bianchini, J. Janek and T. Brezesinski, *Mater. Futures*, 2022, **1**, 015102.
34 S. Wang, W. Zhang, X. Chen, D. Das, R. Ruess, A. Gautam, F. Walther, S. Ohno, R. Koerver, Q. Zhang, W. G. Zeier, F. H. Richter, C.-W. Nan and J. Janek, *Adv. Energy Mater.*, 2021, **11**, 2100654.
35 J. Auvergniot, A. Cassel, D. Foix, V. Viallet, V. Seznec and R. Dedryvère, *Solid State Ion.*, 2017, **300**, 78–85.
36 Y. Xiao, Y. Wang, S.-H. Bo, J. C. Kim, L. J. Miara and G. Ceder, *Nat. Rev. Mater.*, 2020, **5**, 105–126.
37 Y. Han, S. H. Jung, H. Kwak, S. Jun, H. H. Kwak, J. H. Lee, S.-T. Hong and Y. S. Jung, *Adv. Energy Mater.*, 2021, **11**, 2100126.
38 Y. Ma, J. H. Teo, F. Walther, Y. Ma, R. Zhang, A. Mazilkin, Y. Tang, D. Goonetilleke, J. Janek, M. Bianchini and T. Brezesinski, *Adv. Funct. Mater.*, 2022, **32**, 2111829.